The Physical Foundation of Vasoocclusion in Sickle Cell Disease

Alexey Aprelev,[†] William Stephenson,[†] Hongseok (Moses) Noh,[‡] Maureen Meier,[§] and Frank A. Ferrone[†*]
[†]Department of Physics and [‡]Department of Mechanical Engineering and Mechanics, Drexel University, Philadelphia, Pennsylvania; and [§]St. Christopher's Hospital for Children, Philadelphia, Pennsylvania

ABSTRACT The pathology of sickle cell disease arises from the occlusion of small blood vessels because of polymerization of the sickle hemoglobin within the red cells. We present measurements using a microfluidic method we have developed to determine the pressure required to eject individual red cells from a capillary-sized channel after the cell has sickled. We find that the maximum pressure is only ~100 Pa, much smaller than typically found in the microcirculation. This explains why experiments using animal models have not observed occlusion beginning in capillaries. The magnitude of the pressure and its dependence on intracellular concentration are both well described as consequences of sickle hemoglobin polymerization acting as a Brownian ratchet. Given the recently determined stiffness of sickle hemoglobin gels, the observed obstruction seen in sickle cell disease as mediated by adherent cells can now be rationalized, and surprisingly suggests a window of maximum vulnerability during circulation of sickle cells.

Received for publication 26 July 2012 and in final form 6 September 2012.

*Correspondence: fferrone@physics.drexel.edu

Human capillaries are narrower than the erythrocytes they convey. In sickle cell disease, red cells can become rigid in those capillaries, because the hemoglobin inside the red cell will aggregate into stiff polymers. This happens once the molecules deliver their oxygen, and led to the long-held view that capillary occlusion was central to the pathophysiology of the disease (1,2). This was challenged when microscopic study of animal model tissues perfused with sickle blood revealed blockages that began further downstream, in the somewhat larger venules (3–5), at the site of adherent red or white cells which diminished the vessel lumen without fully obstructing the flow. Yet no rationale has been presented for the failure of the prior assumption of capillary blockage. Microfluidic methods (6) are ideally suited to discover why cells don't get stuck in the capillaries, yet occlude subsequent vessels, and we have constructed a system to address this question. Our measurements show that the pressure differences across capillaries in vivo can easily dislodge a cell sickled within a capillary, giving an experimental answer to the question of why sickled cells don't stick in capillaries. It turns out that the pressure a cell can withstand is quantitatively explained by the Brownian ratchet behavior of sickle hemoglobin polymerization.

We constructed single-cell channels in transparent polydimethylsiloxane, with a cross section (1.5 μm $\times$ 4 μm) that is smaller than the resting diameter of red cells (Fig. 1). These channels are much narrower than those that have been employed in other recent studies of the sickling process (7,8), and they resemble human capillaries in permitting only one cell at a time to pass through them. We used a laser photolysis method to create ligand free (deoxygenated) cells, and this requires that the hemoglobin bind CO, which can then be readily removed by strong illumination, in contrast to bound O_2 which is released with far lower efficiency than CO. The microfluidic chips were enclosed in a gas-tight chamber flushed with CO to avoid introduction of oxygen and keep the cells fully ligated before photolysis. The profiles of the channels were confirmed by microscopic observation. To confirm that liquid did not pass around the cells when they were trapped in the channels, fluorescent beads were introduced into some cell solutions. The beads did not pass the cells, nor did they approach the cell when it was occluded, verifying that no significant flow occurred around the cell when it was stuck.

Optical measurements were carried out on a microspectrophotometer constructed on an optical table. The system employed $\times$32 LWD objectives (Leitz, Wetzlar, Germany), which were autofocused during collection of absorption spectra to minimize aberrations. Spectra were obtained using a series 300 camera (Photometrics, Tucson, AZ); video imaging was done with a high-speed camera (Photron, San Diego, CA). Photolysis was provided by a 2020 Argon Ion laser (Spectra Physics, Houston, TX). Sickle cells were obtained from patients at the Marian Anderson Sickle Cell Center at St. Christopher's Hospital for Children, Philadelphia, PA by phlebotomy into EDTA-containing tubes. The blood was centrifuged at 5°C at 1200g for 4 min, and then the pellet was washed 4$\times$ with 15 volumes of buffer (120 mM NaCl, 2 mM KCl, 10 mM dibasic Na Phosphate, 7 mM monobasic Na Phosphate, 3.4 mM Na Bicarbonate, and 6 mM Dextrose) by repeated suspension and centrifugation at 30g for 4 min. This minimizes fibrinogen and platelets in the final suspension, to insure that these studies are controlled by the mechanical properties of the cells themselves.

Editor: David Piston.

http://dx.doi.org/10.1016/j.bpj.2012.09.003

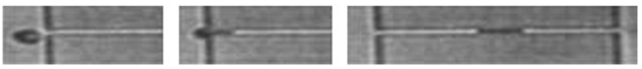

FIGURE 1 An erythrocyte enters a channel (moving *left* to *right*) and is positioned in the center, where it will be photolyzed. The channel cross section is 1.5 μm $\times$ 4 μm, smaller than a resting red cell diameter.

Our experiment began by parking a cell in the center of a channel (Fig. 1). The cell, its hemoglobin, and the microchannel environment all were saturated with CO. Because the thickness of the channel is known, we were able to determine the hemoglobin concentration inside the cell from its absorption spectrum (Fig. 2 *A*). Steady-state laser illumination then removed the CO, allowing the hemoglobin to polymerize, in which condition it remained while the laser was kept on. Removal of CO was confirmed by observing the spectral difference between COHb and deoxyHb. Photolysis of COHb generates negligible heating (9–11). During illumination, hydrostatic pressure was applied until the cell broke free.

The magnitude of the dislodging pressure, measured by simple height difference between input and output cell reservoirs, is shown in Fig. 2 *B*. The pressure needed to dislodge the cell increased with increasing intracellular Hb concentration, implying that an increased mass of polymerized hemoglobin is more difficult to dislodge. A clear concentration threshold for capture is apparent. While there is a well-known solubility below which polymers cannot form (18.5 g/dL for the 22°C of this experiment (12)), the threshold here is significantly higher.

Central to explaining these observations is a Brownian ratchet mechanism (13) which derives from the metastable nature of this polymerization process. Unless disrupted, as by centrifugation, polymerization in sickle hemoglobin terminates before the thermodynamic limit of monomer solubility is reached (14,15). This arises from the fact that polymers only grow at their ends, which are easily occluded in the dense mass of polymers that form. This end obstruction leaves the system in a metastable state and fluctuations accordingly provide polymers with space into which they can incrementally grow. This Brownian ratchet has been shown to lead to dramatic fiber buckling when individual fibers are isolated in sickle cells (16). The force can be simply expressed as $f = (kT/\delta)\ \ln\ S(c)$, where k is Boltzmann's constant, T the absolute temperature, δ the net spatial elongation from addition of a single monomer, and S is the supersaturation of the solution when the metastable limit is reached, at monomer concentration c. In this calculation, c is taken as the terminal concentration, computed from our empirical finding (15) that in this metastable system the amount of polymerized hemoglobin Δ is $\Delta(\infty) = 2/3\ (c_o\text{-}c_s)$, rather than the expected thermodynamic limit $c_o\text{-}c_s$, where c_o is the initial concentration and c_s is the solubility.

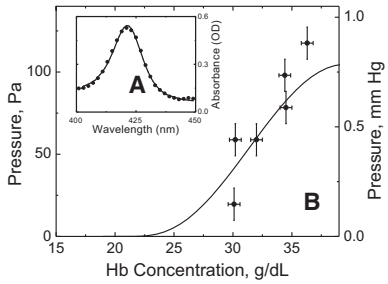

FIGURE 2 (*A*) Absorption of the cell (points), fit to a standard spectrum (9). (*B*) Pressure to dislodge a cell sickled in the microchannel, as a function of intracellular concentration. Note that typical intracellular concentrations are ~32 g/dL. (*Line*) Brownian-ratchet theory described in the text. The coefficient of friction (0.036) is within the observed range, and is the only parameter varied.

For determining the net force, the total number of fibers must be known, and can be calculated based on the double nucleation mechanism (17) which has been quantitatively successful in describing polymerization. The concentration of polymers $[p(t)]$ initially grows exponentially, described by

$$[p(t)] = \left(\frac{AB}{2J}\right)\ \exp(Bt),$$

where A and B are parameters related to nucleation, and J is the polymer elongation rate, as described in Ferrone et al. (17). Because A and B are both extremely concentration-dependent (9), they will drop dramatically once monomers begin to add to polymers in any significant numbers, and thereby diminish the remaining monomer pool. Thanks to the extreme concentration dependence of the reaction, this rapidly shuts off further polymerization. This happens at approximately the 10th time (the time when the reaction has reached 1/10 of its maximum). Thus, the $[p(t_{1/10})] \approx [p(\infty)]$. Moreover, at one-tenth of the reaction,

$$\Delta\left(t_{1/10}\right) = \frac{1}{2}A\ \exp\left(Bt_{1/10}\right) = \frac{\Delta(\infty)}{10},$$

and thus

$$[p(\infty)] = \left(\frac{B}{J}\right)\left(\frac{\Delta(\infty)}{10}\right) = \left(\frac{B}{J}\right)\left(\frac{(c_o - c_s)}{15}\right).$$

For computing the number of fibers, the volume of the cell was taken as 90 μm^3. This calculation shows, as expected, that the number of polymers in the cell is highly concentration-dependent, and very few fibers are produced at concentrations just above solubility, but the number grows sharply as concentration rises. This is the main contribution to the threshold in holding force shown by the data.

With the force per fiber, and the total number of fibers, the net force against the wall is known. With a coefficient of friction, this reveals the force that a trapped cell can withstand. If the force is divided by the cross-sectional area across which

the force is applied, we get a prediction of the dislodging pressure, which can be compared to the data. For a quantitative comparison with the results, two further corrections, of order unity, were applied. Because only normal force will contribute to friction, the calculated force was determined by integrating cos θ. This integration is not over all angles (π) because of the possibility that large incidence angles of the fibers against the wall will lead to fiber runaway (18). Therefore, the integration described is taken to the runaway threshold, here ~1 rad. Finally, it is necessary to assign a coefficient of friction. Known values span the range of 0.03–0.06 (19). We therefore selected a value within the range, 0.036, as the best match for the data. The predicted pressures match the measurements well, as the line in Fig. 2 *B* shows.

Because the flow resistance is comparable for red cells traversing glass channels and endothelial-lined capillaries (20), we conclude that in vivo the pressures a sickled cell inside a capillary can withstand are no more than hundreds of Pa. This is significantly smaller than typical arteriovenous pressure differentials that have been measured, which range from 0.7 kPa (in hamster skin (21)) to 7.9 kPa (in rat mesentery (22)).

Our measurements coupled with recent determination of the stiffness of sickle hemoglobin gels (23) provide the missing physical basis for the processes of vasoocclusion seen in ex vivo tissue and animal models of sickle cell disease, arguing that these observations indeed represent fundamental behavior of sickle cell disease. We now understand this behavior in terms of three possible outcomes, all intimately connected with kinetics:

1. Certain escape: A cell that does not polymerize until after passing the obstruction can reach the lungs where it reoxygenates and resets its polymerization clock.
2. Possible escape: A cell that polymerizes within the capillary will assume an elongated sausage shape. The forces that it can exert against the wall cannot hold it there, and it will emerge into the postcapillary venule. There it has some chance of passing a subsequent obstruction, though it might also obstruct flow were it to rotate before reaching the adherent cell, so as to present its long dimension to the reduced space it must traverse.
3. Certain occlusion: A cell that does not polymerize in the capillary reassumes a larger diameter as soon as it escapes. If the cell then polymerizes before it encounters a cell attached to the venule wall, this rigidified cell will not be able to squeeze past the adherent cell, because that kind of deformation takes MPa (23). This would precipitate the type of blockage that is observed. This suggests that there is a window of greatest vulnerability, toward which therapies might be addressed.

ACKNOWLEDGMENTS

We thank the NHLBI of the NIH for their support.

REFERENCES and FOOTNOTES

1. Eaton, W. A., J. Hofrichter, and P. D. Ross. 1976. Editorial. Delay time of gelation: a possible determinant of clinical severity in sickle cell disease. *Blood.* 47:621–627.
2. Eaton, W. A., and J. Hofrichter. 1987. Hemoglobin S gelation and sickle cell disease. *Blood.* 70:1245–1266.
3. Kaul, D. K., M. E. Fabry, and R. L. Nagel. 1989. Microvascular sites and characteristics of sickle cell adhesion to vascular endothelium in shear flow conditions: pathophysiological implications. *Proc. Natl. Acad. Sci. USA.* 86:3356–3360.
4. Kaul, D. K., M. E. Fabry, …, R. L. Nagel. 1995. In vivo demonstration of red cell-endothelial interaction, sickling and altered microvascular response to oxygen in the sickle transgenic mouse. *J. Clin. Invest.* 96:2845–2853.
5. Frenette, P. S. 2004. Sickle cell vasoocclusion: heterotypic, multicellular aggregations driven by leukocyte adhesion. *Microcirculation.* 11:167–177.
6. Hersher, R. 2012. Microfluidic chips promise better diagnosis for sickle cell disease. *Nat. Med.* 18:475.
7. Higgins, J. M., D. T. Eddington, …, L. Mahadevan. 2007. Sickle cell vasoocclusion and rescue in a microfluidic device. *Proc. Natl. Acad. Sci. USA.* 104:20496–20500.
8. Wood, D. K., A. Soriano, …, S. N. Bhatia. 2012. A biophysical indicator of vaso-occlusive risk in sickle cell disease. *Sci. Transl. Med.* 4:123ra126.
9. Ferrone, F. A., J. Hofrichter, and W. A. Eaton. 1985. Kinetics of sickle hemoglobin polymerization. I. Studies using temperature-jump and laser photolysis techniques. *J. Mol. Biol.* 183:591–610.
10. Hofrichter, J. 1986. Kinetics of sickle hemoglobin polymerization. III. Nucleation rates determined from stochastic fluctuations in polymerization progress curves. *J. Mol. Biol.* 189:553–571.
11. Galkin, O., R. L. Nagel, and P. G. Vekilov. 2007. The kinetics of nucleation and growth of sickle cell hemoglobin fibers. *J. Mol. Biol.* 365:425–439.
12. Ross, P. D., J. Hofrichter, and W. A. Eaton. 1977. Thermodynamics of gelation of sickle cell deoxyhemoglobin. *J. Mol. Biol.* 115:111–134.
13. Daniels, D. R., and M. S. Turner. 2004. The force generated by biological membranes on a polymer rod and its response: statics and dynamics. *J. Chem. Phys.* 121:7401–7407.
14. Aprelev, A., W. Weng, …, F. A. Ferrone. 2007. Metastable polymerization of sickle hemoglobin in droplets. *J. Mol. Biol.* 369:1170–1174.
15. Weng, W., A. Aprelev, …, F. A. Ferrone. 2008. Universal metastability of sickle hemoglobin polymerization. *J. Mol. Biol.* 377:1228–1235.
16. Daniels, D. R., J. C. Wang, …, M. S. Turner. 2006. Deforming biological membranes: how the cytoskeleton affects a polymerizing fiber. *J. Chem. Phys.* 124:024903.
17. Ferrone, F. A., J. Hofrichter, and W. A. Eaton. 1985. Kinetics of sickle hemoglobin polymerization. II. A double nucleation mechanism. *J. Mol. Biol.* 183:611–631.
18. Daniels, D. R., D. Marenduzzo, and M. S. Turner. 2006. Stall, spiculate, or run away: the fate of fibers growing towards fluctuating membranes. *Phys. Rev. Lett.* 97:098101.
19. Dunn, A. C., T. D. Zaveri, …, W. G. Sawyer. 2007. Macroscopic friction coefficient measurements on living endothelial cells. *Tribol. Lett.* 27:233–238.
20. Pries, A. R., T. W. Secomb, …, P. Gaehtgens. 1997. Microvascular blood flow resistance: role of endothelial surface layer. *Am. J. Physiol.* 273:H2272–H2279.
21. Cabrales, P., A. G. Tsai, and M. Intaglietta. 2004. Microvascular pressure and functional capillary density in extreme hemodilution with low- and high-viscosity dextran and a low-viscosity Hb-based O_2 carrier. *Am. J. Physiol. Heart Circ. Physiol.* 287:H363–H373.
22. Pries, A. R., T. W. Secomb, …, P. Gaehtgens. 1994. Resistance to blood flow in microvessels in vivo. *Circ. Res.* 75:904–915.
23. Zakharov, M. N., A. Aprelev, …, F. A. Ferrone. 2010. The microrheology of sickle hemoglobin gels. *Biophys. J.* 99:1149–1156.